Contrib Mineral Petrol (2002) 143: 300–315
DOI 10.1007/s00410-002-0351-z

Catherine Ginibre · Gerhard Wörner · Andreas Kronz

Minor- and trace-element zoning in plagioclase: implications for magma chamber processes at Parinacota volcano, northern Chile

Received: 21 February 2001 / Accepted: 7 January 2002 / Published online: 22 March 2002

Abstract Textural and compositional zoning in plagioclase phenocrysts in a sample from Parinacota volcano (Chile) was investigated using backscattered electron images and electron microprobe analysis of major and trace elements. Large (2 mm) oscillatory zoned crystals (type I) with resorption surfaces of moderate An discontinuities ($\leqslant 10\%$ An) and decreasing trace-element contents (Sr, Mg, Ti) towards the rim reflect melt differentiation and turbulent convection in the main magma body. Early recharge with a low-Sr mafic magma is seen in the core. Small-scale Sr variations in the core indicate limited diffusion and thus residence and differentiation times of the magma shorter than a few thousand years. Smaller crystals (type II) with low trace-element/An ratio reflect the influence of an H_2O-rich melt probably from a differentiated boundary layer. Closed-system in-situ crystallisation, mafic magma recharge and the role of a water-rich differentiated boundary layer can be distinguished from the An–trace element relationships. Crystals apparently move relatively freely between different parts and regimes in the magma chamber, evidence for "convective crystal dispersion". High-Sr type II crystals indicate an earlier input of Sr-rich mafic magma. Recharge of two distinct mafic magma types is thus identified (high-Sr and low-Sr), which must have been present – at increasing recharge rates with time – in the plumbing system throughout the volcano's history.

C. Ginibre (✉) · G. Wörner · A. Kronz
Geowissenschafliches Zentrum Göttingen,
Abt. Geochemie, Goldschmidtstr. 1,
37077 Göttingen, Germany
E-mail: catherine.ginibre@chimie.univ-nantes.fr
Fax: +330251125268

Present address: C. Ginibre
Laboratoire de Planétologie et Géodynamique,
Université de Nantes, Faculté des Sciences et des Techniques,
2 rue de la Houssinière, BP 92208,
44322 Nantes cedex 3, France

Editorial responsibility: T.L. Grove

Introduction

Magma chamber processes play an important role in the formation of igneous rocks and include crystal growth, bulk melt differentiation, convection, magma recharge and other processes depending on dynamic and thermal regimes. Experimental and numerical models of magma chamber processes (see reviews and discussion in Marsh 1989a, 1989b, and Huppert and Turner 1991) allow to constrain the role of physical parameters such as density and viscosity as a function of melt composition, temperature gradients, geometry of the magma chamber, etc. However, such models are difficult to apply directly to natural systems because many of these parameters are not well constrained.

A complementary approach uses records of the crystallisation history in volcanic products, such as zoning in plagioclase. Due to sluggish diffusion of the Si–Al pair in plagioclase (Grove et al. 1981), major-element zoning reflecting the An–Ab binary system has been widely used in studying igneous plagioclase as a record of magma compositions and crystallisation conditions. Petrographic observation and high-resolution imaging methods (e.g. laser interference and Nomarsky interference; Anderson 1983, 1984; Pearce et al. 1987; Nixon and Pearce 1987) have also been applied. Experimental studies of crystallisation (Lofgren 1974) and resorption (Tsuchiyama 1985; Johannes et al. 1994; Nakamura and Shimakita 1998) or numerical modelling (Allègre et al. 1981; Loomis 1982; Lasaga 1982; L'Heureux and Fowler 1996) provided insights into the kinetics of plagioclase growth and resorption.

Although these studies have brought a better understanding of the origin of zoning patterns, limitations remain from insufficient spatial resolution of imaging and chemical analysis, as well as from the fact that the effects of several factors (P, T, melt composition, H_2O content) on the An–Ab system cannot be distinguished.

In order to address the latter problem, several recent studies have combined textural imaging with minor- and

trace-element analyses by SIMS (Blundy and Shimizu 1991; Singer et al. 1995; Brophy et al. 1996) or isotopic data (Davidson and Tepley 1997; Tepley et al. 2000). This combination allowed to better identify the causes of plagioclase zoning patterns, for example, recharge and assimilation. However, because of the low spatial resolution of SIMS and microdrilling (a few tens to hundreds of microns) and the large efforts and costs involved, this approach does not allow the study of zoning at small scale for a large number of samples. Despite lower precision, electron microprobe analysis has the advantage of a much better spatial resolution (a few μm). Kuritani (1998), for example, analysed several distinct zones in a large number of plagioclase crystals for major and minor (Fe, Mg) elements using the electron microprobe. He reconstructed specific locations of plagioclase growth within the magma chamber of the Rishiri volcano (Japan). He was able to distinguish plagioclase that originated from the chamber's boundary layer at the wall rock from those of the magma body.

In the present study we analysed plagioclase phenocrysts from a dacite from the Upper Pleistocene to Holocene Parincota volcano of the Central Andean Volcanic Zone (northern Chile). We used an electron microprobe for minor and trace elements with a spatial resolution of a few microns. The trace-element data are combined with textural observations using BSE images (Ginibre et al. 2002). We distinguish between the role of the crystal-chemical influence on the partition coefficients of minor and trace elements, diffusion in the crystal, bulk melt composition (X, H_2O content, fO_2), kinetic effects at the crystal–melt interface, and variation of intensive parameters (T, P). This approach provides evidence for several processes: compositional differentiation, magma recharge of two distinct mafic magmas with and without chemical mixing, as well as crystallisation in an H_2O-enriched magma chamber boundary layer.

Samples and methods

Samples

Parinacota is an Upper Pleistocene to Holocene volcanic complex in the Central Volcanic Zone of the Andes. Sample PAR-130 studied here is a dacite (66.83 wt% SiO_2, Table 1) belonging to the old stratocone stage (eruptive stage IIa, 53,000–18,000 years; Wörner et al. 1988, 2000). This "Old Cone" stage is characterised by a large compositional range (mafic andesites to rather porphyric silicic andesites, dacites and rhyolites). This period had an extended differentiation history with low eruption rates and mixing between mafic magmas and older dacitic to rhyolitic magmas. In an Ni–Rb diagram (Wörner et al. 1988), Parinacota Old Cone whole-rock concentrations fall on mixing lines between mafic and differentiated end members. A catastrophic collapse around $18{,}150 \pm 650$ years (Wörner et al. 2000) was followed by the rapid eruption of mafic to intermediate andesites and the rebuilding of the "New Cone" ($< 18{,}000$ to about 2,000 years). This new "healing" stage represents a sudden change from low eruption rates and large compositional variations to high eruption rates and lavas with a more restricted compositional spectrum. Two distinct mafic magmas, the one with low, the other with high Sr (and Ba) concentrations were erupted in a final stage in flanc eruptions (Ajata flows). The overall compositional variation of Parinacota lavas suggests that these two types of mafic magma may be involved in recharge events and mixing (Wörner et al. 1988; Davidson et al. 1990).

Table 1. Composition of sample PAR-130. Major element concentrations are in wt %: trace element concentrations are in ppm

	PAR-130
SiO_2	66.83
TiO_2	0.65
Al_2O_3	16.05
FeO*	3.6
MnO	0.06
MgO	1.26
CaO	3.33
Na_2O	4.07
K_2O	3.89
P_2O_5	0.26
Total	100.00
V	61
Cr	8
Co	30
Ni	16
Cu	27
Zn	83
Rb	152
Sr	664
Y	15
Zr	218
Nb	11
Ba	1,172

Sample PAR-130 was chosen for its relatively simple petrography, which should allow us to better identify individual processes. PAR-130 contains ca. 15% plagioclase (An_{55}–An_{30}), 5% euhedral phenocrysts of ortho- and clinopyroxene, below 1% euhedral hornblende and rounded biotite, two iron-titanium oxides, and a matrix composed of pyroxene, apatite, oxide, K-feldspar microcrysts and glass. Most other Old Cone Parinacota andesitic to dacitic samples contain rounded sanidine and quartz xenocrysts as well as rhyolitic plagioclase (An_{40} to An_{20}) with fine and extensive sieve textures at the rim, which is typical evidence for late magma mixing. By contrast, plagioclase phenocrysts from PAR-130 show no resorption at the rim, and the rock contains neither sanidine nor quartz xenocrysts. PAR-130 has low Ni and high Rb values, similar to the rhyolites from Parinacota eruptive stages Ia, i.e. it is close to the differentiated end member.

Methods

After petrographical examination, selected crystals were investigated with a JEOL 8900 RL electron microprobe.

BSE imaging

Zoning patterns were documented by back-scattered electron (BSE) images where BSE intensity in plagioclase corresponds to An content. BSE intensity profiles were calibrated for An content using quantitative point analyses following the approach described by Ginibre et al. (2002).

Quantitative point analyses

Quantitative point analyses for Al, Si, Na, Ca, K, Ba, Sr, Fe, Ti and Mg were performed at 20-kV acceleration voltage and 40-nA beam current, with 2- or 5-μm beam size. Alkali elements were analysed first, and all major elements were analysed during the first 90 s (16-s counting time on peak). A study of Na loss shows that alkalis were not significantly lost during this time period. Minor (Ba, Sr and Fe) and trace elements (Ti, Mg) were then analysed over 4-min counting time on the peak. The influence of alkali loss on the minor and trace elements is small enough to be negligible because, for these elements, the intensity/count ratio is constant and independent of minor variations in major-element composition. Table 2 lists the detection limits for Ba, Sr, Fe, Mg, and Ti, as well as the ranges of concentrations and statistical errors ($\pm 2\sigma$) for the analyses at the concentrations measured.

The spatial resolution of wavelength-dispersive (WDS) analysis is a few microns. In homogeneous zones, no significant differences were found between analyses with a 2- and a 5-μm beam. Particular attention was given to measuring clear, homogeneous zones. Whenever the size of fine patchy or oscillatory zoning is below the WDS spatial resolution, the reported analyses represent an average over these heterogeneities. After measurement, the points are viewed and precisely located on BSE or secondary electron (SE) images, and can thus be related to the type and width of the An zoning. Measurement points were subsequently examined under the optical microscope in order to eliminate data points too close to inclusions.

This has been done in particular because secondary fluorescence of iron-rich phases located near the measured feldspars may influence measured Fe content in plagioclase (Longhi et al. 1976). None of the measurements presented here is closer than 50 μm to iron-rich phases (oxide, pyroxene, etc). The influence of the matrix, which contains less than 1 wt% FeO, is below the analytical uncertainty (70 ppm) and can be neglected. Iron concentrations were therefore not corrected for secondary fluorescence effects at the rims of the crystals.

Zoning patterns in PAR-130 plagioclase phenocrysts

The diversity of plagioclase zoning patterns in sample PAR-130 is shown in Fig. 1. We distinguish two types of plagioclase phenocrysts: type I crystals are 1–4 mm large and oscillatory zoned with only weak resorptions as described below. This type comprises a relatively small proportion of crystals, which represent over half of the plagioclase population in volume. Type II crystals are smaller (500 μm to 1.5 mm) and more extensively resorbed. The outer 100 to 200 μm of the larger crystals of both types I and II show oscillatory zoning with rounded edges, similar to numerous microphenocrysts.

Type I crystals

Three representative type I crystals (P1, P3 and P4) were chosen for detailed investigation. They all have similar overall zoning patterns in major and minor elements. BSE An-calibrated and quantitative profiles were performed in P1 and P4, and in more detail in P3. Patchy growth zones with glass inclusions, which are related to, and grew subsequently to, distinct resorption surfaces are here referred to as resorption zones. These were analysed in detail in P1 and P4.

An content

BSE images and An-calibrated profiles of the analysed crystals are shown in Fig. 2. The three crystals exhibit an overall normal zoning pattern (An_{50} to $An_{30–35}$), with oscillations superimposed on this trend. Details of the oscillatory zoning in plagioclase P3 from sample PAR-130 using high-resolution BSE images are described elsewhere (Ginibre et al. 2002). The following types of zoning are distinguished.

1. Saw-tooth patterns with resorption (STR) are 5 to 20 μm in wavelength, have 5–10 mol% An variations, and are separated by wavy surfaces (“r” in Fig. 3). These patterns are interpreted to result from growth interruption and minor resorption of the last grown layer.

Table 2. Detection limits and ranges of concentration for Mg, Ti, Fe, Sr and Ba in sample PAR-130 (all values are given in ppm)

	Mg	Ti	Fe	Sr	Ba
Detection limit[a]	17	18	29	67	50
Concentration range	100–250	100–400	1,000–4,000	1,000–3,000	500–2,000
Statistical error[b]	19	28–31	60–70	110–120	70–75

[a]Calculated as 2× standard deviation of the intensity at background position ($n = 97$, 95% confidence level)
[b]Calculated from counting statistics for each analysis

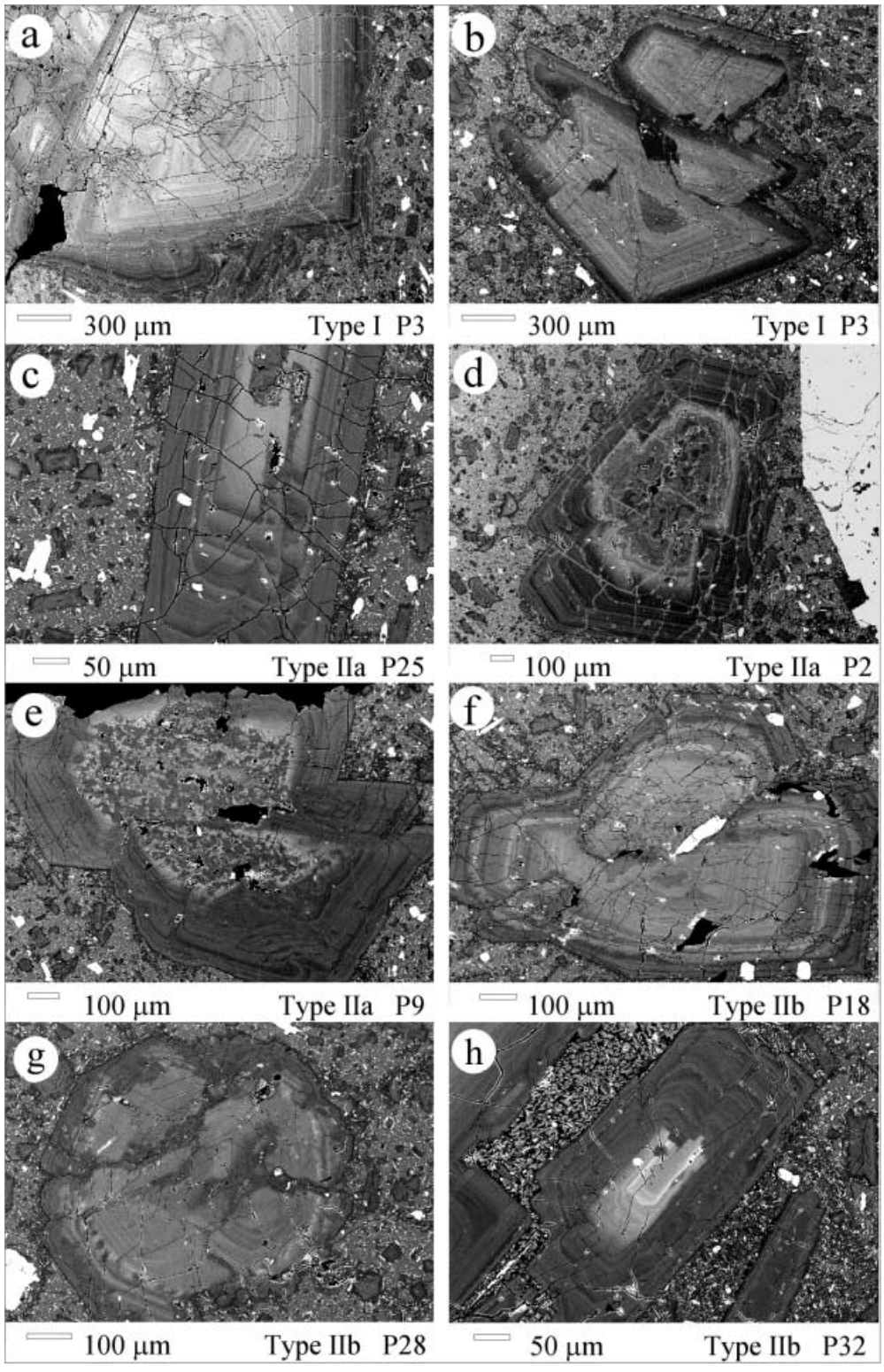

Fig. 1a–h. Crystal types of plagioclase in PAR-130. **a** P3 is typical for type I (large oscillatory zoned) crystals. Type II crystals show more resorption or more contrast between core and rim. **b–e** Images of type IIa crystals P42, P25, P2, and P9. **f–h** Images of type IIb crystals P18, P28, and P32. The latter are distinguished only on the basis of their Sr contents (see Fig. 6)

2. Low-amplitude oscillations (LAO) at 1-μm wavelength and 1% An variation are superimposed on normal zoning of the STR zones and are most likely due to local kinetic control. These are not considered further in the present study.
3. Major resorption surfaces (R) with discontinuities in An content up to 10% An crosscut several growth layers (STR and LAO). Some of these resorption surfaces form bands containing glass inclusions and patchy zoning, referred to as resorption zones (Fig. 3).

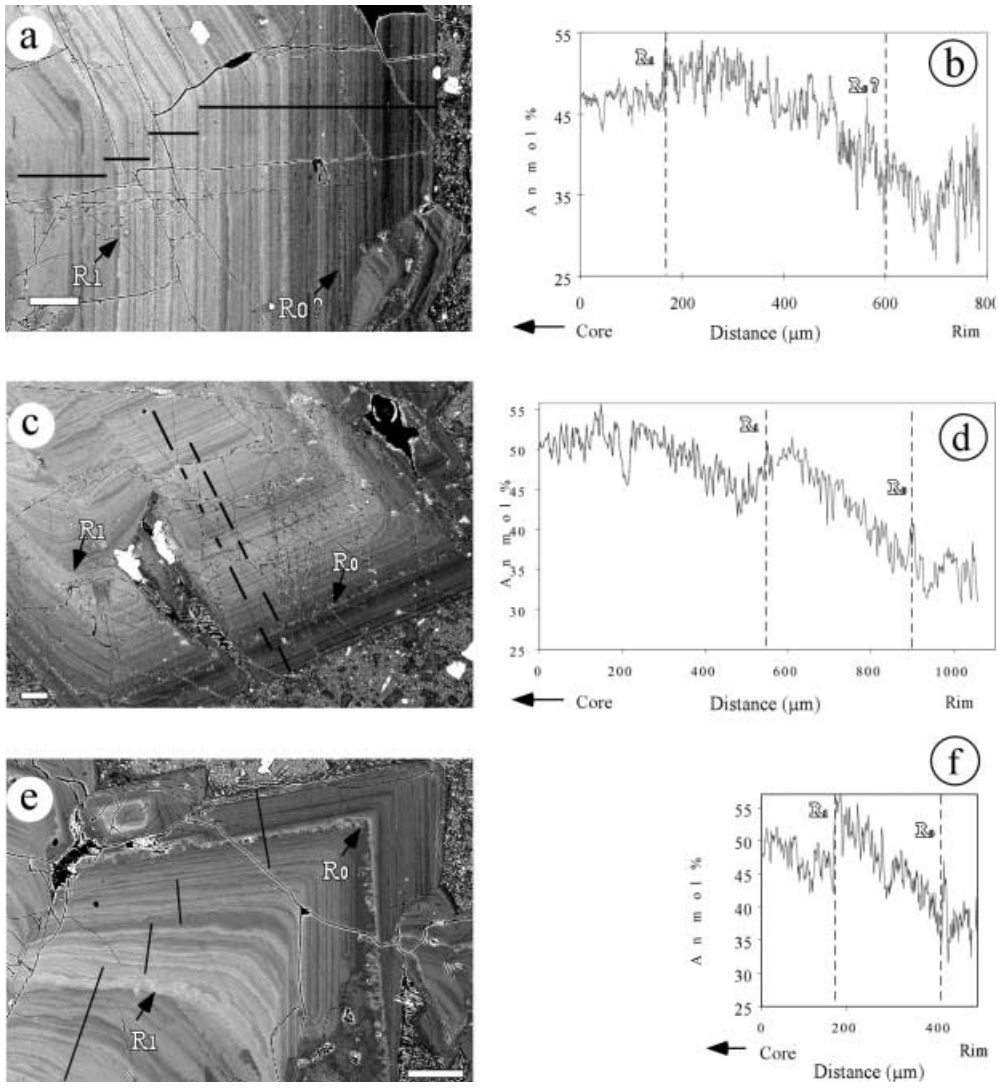

Fig. 2a–f. BSE image of type I plagioclase crystals PAR-130-P3, P4, and P1. *Scale bar* is 100 μm for all crystals and profiles. An-calibrated profiles through BSE images are shown for each crystal. For P3, the profile from high-resolution accumulated image (Ginibre et al. 2002) is shown. For P1 and P4, profiles are taken from the image along the lines. R_0 is a prominent, important resorption surface late in the crystallisation history. It can be correlated between P4 and P1, and probably corresponds to the boundary between zones 7 and 8 in P3 (see Fig. 4). R_1 is a resorption surface with an An peak near the core, and probably represents the same event in the three crystals (see discussion in text)

4. High-frequency (3 μm) An variations with high amplitudes (10 mol% An; HFA) at the rapidly grown, outer crystal margin are interpreted as an extreme form of STR due to increased dynamic movements of crystals and melt during eruption.

Special cases are the complex, patchy resorption zones representing three stages of plagioclase growth. (1) The last zone grown before resorption (Pl_1 on Fig. 3b) is generally sodic ($An_{30–40}$). The resorption surface itself is irregular and penetrates deeply into this zone. (2) A calcic zone (Pl_2, $An_{50–60}$) is located directly at the resorption surface and is similar to those observed in partial melting experiments (Tsuchiyama 1985; Johannes et al. 1994; Nakamura and Shimakita 1998; Hammouda and Pichavant 2000). They therefore may be interpreted as having grown during or directly after partial dissolution of the more sodic crystal. (3) New sodic zones ($An_{30–40}$) sometimes exhibit oscillations and occur around the inclusions. These zones are chemically identical to the next outer growth layer, which crystallised after the resorption event, and are therefore interpreted to be simultaneous to further growth at the outer rim of the crystal. Individual zones are often too small ($\leqslant 5$ μm) to be measured separately, and point analyses are therefore mixed between a sodic and a calcic end member.

Direct correlation of zoning patterns between P1, P3 and P4 is not possible. There are, however, several striking similarities between crystals. An An maximum is observed near the core, followed by a general decrease from An_{50} to minimum of An_{30} and a slight An increase towards the rim. The last three STR zones in crystals P1, P4 and P3 are very similar in size, morphology and compositional range, and may thus be correlated. The last resorption zone can also be correlated between P1 and P4, having similar composition and morphology. They also are located directly before the An minimum in the profile. It will be referred to as R_0 for P1 and P4 in the following. Such an R_0 resorption zone is difficult to identify in P3, but might be represented by the resorption zone between growth zones 7 and 8.

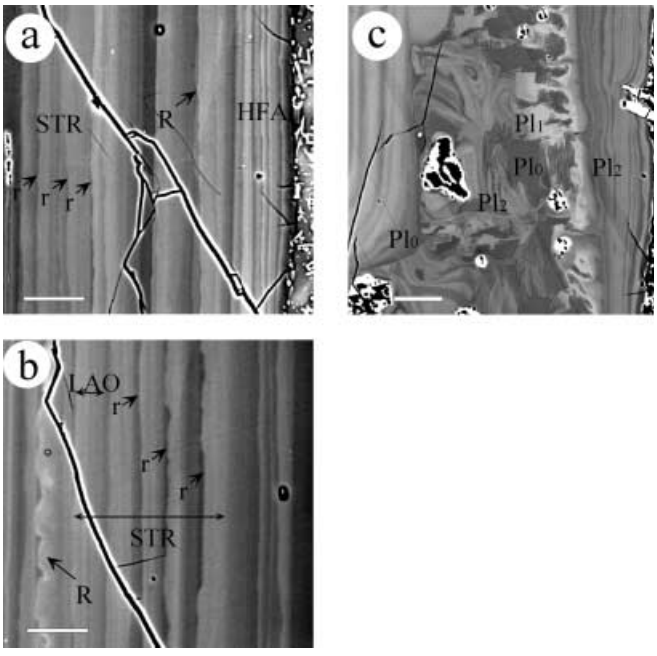

Fig. 3a–c. Details of zoning patterns in plagioclase. *Scale bar* is 20 μm. **a, b** Oscillatory zoning including STR patterns with minor (*r*) and major (*R*) resorption surfaces and superimposed *LAO* oscillations, as well as *HFA* oscillations at the rim (Ginibre et al. 2002). **c** Patchy zoning at the resorption surface R_0 in crystal P1. Pl_0 represents remnant plagioclase grown before resorption. Pl_1 is the plagioclase grown during or immediately after resorption. Pl_2 is the plagioclase grown in the following growth phases, both in the melt inclusion and outward from the resorption zone

Differences between the crystals are the variable amplitude and sharpness of the An peaks as well as the number and morphologies of R surfaces and the distance of the R_1 resorption surface to the rim. This variable distance may reflect different degrees of resorption and growth rates. In P3, where zones boundaries are broadly euhedral, the peak and resorption R_1 are at 500 μm from the rim. On the contrary in P1, where the resorption surfaces are more rounded between R_1 and R_0, presumably showing a higher degree of resorption, the same (?) R_1 surface is only 300 μm from the rim.

Minor and trace elements

Based on zoning patterns and composition, we define ten distinct growth zones in crystal P3, which are separated by major resorption surfaces (R, Fig. 4). These growth zones are also distinguished by discontinuities in their anorthite–trace element trends (Fig. 5). High-resolution ($\leqslant 5$ μm) trace-element profiles across the crystal PAR-130-P3 show a general decrease of Sr, Fe, Ti, and Mg from core to rim, and an increase in Ba. In the core (first 100 μm, zone 1), local minima for Ti and Sr are observed. In the outer 50 μm (zone 10) Fe, Ti, Mg and Ba contents increase whereas Sr content decreases. The 5–20 μm oscillations in An content (STR) are not reproduced in trace- and minor-element zonations. This may simply be due to the higher analytical uncertainty for trace elements. Only Fe shows strong oscillations, and only at the outermost rim (Fig. 2b).

Figure 5 combines the data of P3 with those of the two other plagioclase crystals PAR-130-P1 and PAR-130-P4. They exhibit the same general trend from core to rim as P3, except for the resorption zones, not analysed in P3. The composition of the core (inwards from R_0) and rim (outwards from R_0) of P1 and P4, compared to those of P3, confirms that this surface separating zones 7 and 8 could be an equivalent of R_0 in P1 and P4.

At the scale of the whole crystal, Sr, Fe, Ti, Mg are roughly positively correlated with An content, with concentrations high in the core and low in the outer 300 μm (500 to 800 μm from the core). Ba correlates negatively with An.

In the inner zones (1 to 5), Fe, Ti, and Sr contents do not correlate well with An content. Fe is fairly constant at variable An whereas Ti is negatively correlated with An in zones 1 and 2, as is Sr in zone 2. Thus, the overall variation of An content with trace elements (Fig. 5) reflects igneous differentiation of the host melt(s).

In detail, however, there is more structure to this variation. Growth zones 6–7 and 8–9 define parallel linear trends in the An–trace element diagram (Fig. 5). This is particularly well documented for Sr, Fe, and less obvious for Ti. From one growth zone to the next, there are discontinuities in the overall decreases in trace elements. For Ba, a complex pattern is superimposed on the strong overall negative correlation. Mg, by contrast, shows a fairly linear positive correlation with An.

The outermost zone with HFA oscillations in An (zone 10) shows negative correlations of Fe, Ba and Ti with An content, and an increase in Mg compared to zone 9 at similar An content. Sr is negatively correlated with An.

An content in resorption zone R_0 is variable but Fe, Ti, Sr and Mg are fairly constant at low levels. The compositions of the resorption zone in fact fall into a triangular-shaped field in the An–trace element plots. Some data may reflect mixed analyses due to the fine zonations (An-rich resorption zones and subsequent sodic growth) whereas other analyses clearly fall below the differentiation trend, and therefore reflect growth of a high-An plagioclase with low trace-element contents. Only Ba does not show compositional differences between growth and resorption zones.

Type II crystals

Zoning patterns in type II crystals are more variable than in type I, as shown on Fig. 1. Many of them exhibit a resorbed core with a relatively wide, often oscillation-free An-rich zone (P25, P2, P31). Oscillatory zoning with frequent rounded resorption (P18), and small An-rich cores with microphenocryst-like sodic rim (P32) are also observed.

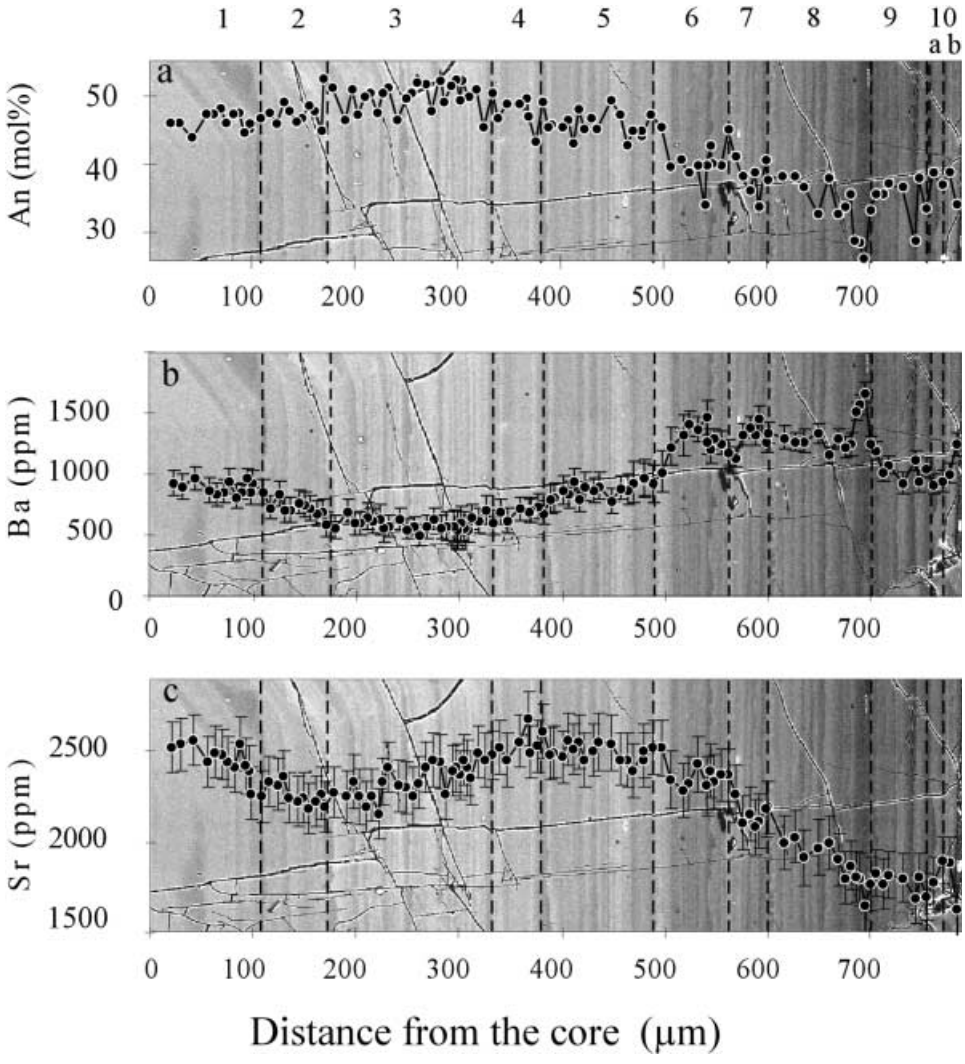

Fig. 4. EMP quantitative point analysis profile of plagioclase PAR-130-P3 from core to rim for An (in mol%), and Ba, Sr, Fe, Ti and Mg (in ppm). The ten distinct growths zones shown here are separated by major resorption surfaces (see Fig. 3 for details) and distinguished on Fig. 5 using the trace-element content

Sr, Fe, and Mg in type II plagioclase are plotted against An in Fig. 6. These crystals all have lower Fe and Mg at variable An compared to type I crystals, but they fall in the field of the R_0 resorption zone. Sr concentrations are variable and we distinguish two subtypes: in type IIa, as for Fe and Mg, Sr is low at high An content, similar to the R_0 zones of type I crystals. On the contrary, type IIb crystals have high Sr concentrations in the core, significantly higher than in the cores of type I crystals (up to 3,800 ppm compared to 2,600 ppm). Types IIa and IIb are not distinguishable on the basis of major-element zoning, and there also exist intermediate compositions between IIa and IIb, with type IIa being more common than type IIb.

Processes controlling major- and trace-element zoning

We first discuss in detail the various factors controlling zoning patterns, applied to the type I crystals, which are believed to record the conditions of crystallisation of the main magma body. We then discuss the additional information provided by the type II crystals.

Control on major elements

Major-element composition of plagioclase is controlled by phase relations and thus gives a general idea of the history of T–P–H_2O conditions of the magma in which the crystals formed. The general An decrease from core to rim can be related to differentiation of the magma. This is more pronounced in the outer 300 μm of PAR-130-P3. By contrast, higher average An contents in zone 3 suggest either a more mafic composition of the melt or higher water content.

Resorption textures very similar to those observed here have been produced experimentally by heating (Johannes et al. 1994), chemical disequilibrium (Tsuchiyama 1985; Nakamura and Shimakita 1998; Hammouda

Fig. 4. (Contd)

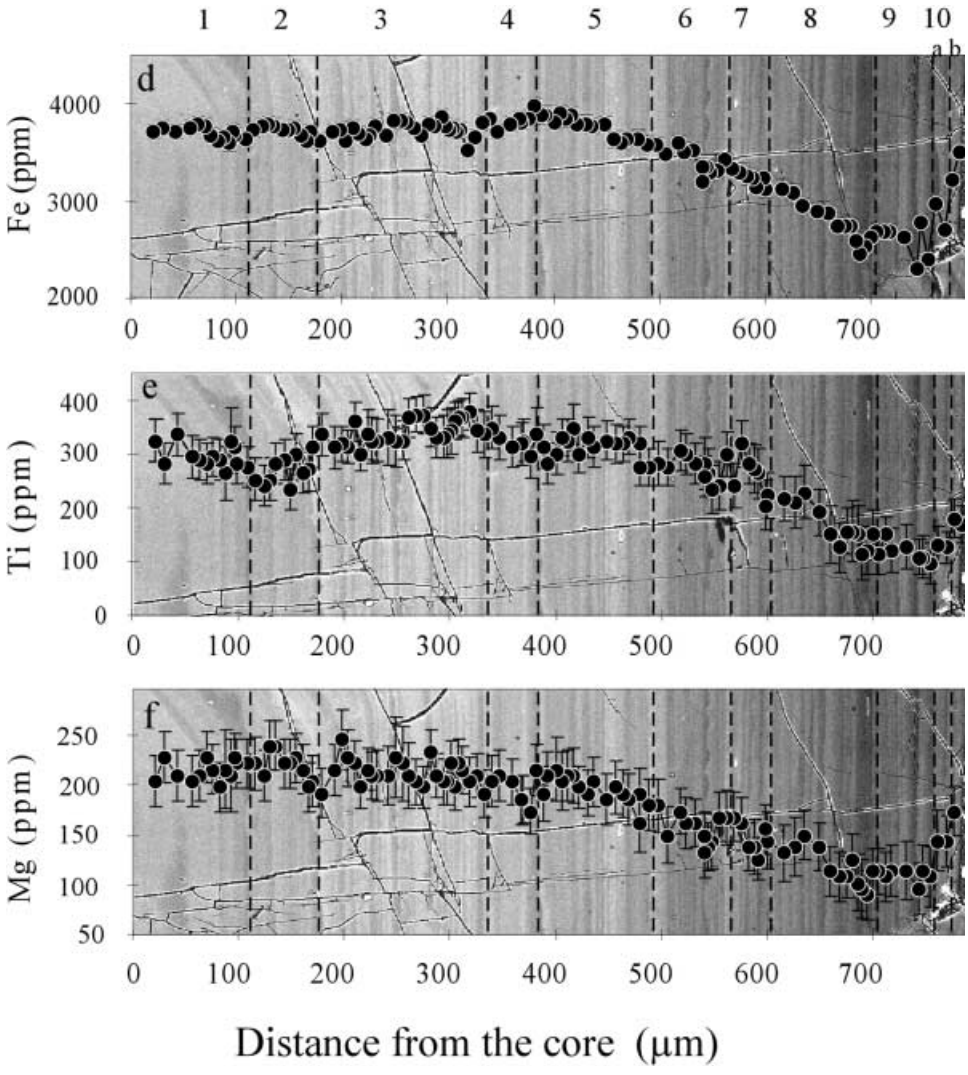

and Pichavant 2000), and decompression (Nelson and Montana 1992). The effect of pressure on plagioclase composition is small (20 mol% An for 12 kbar) compared to that of temperature (Housh and Luhr 1991). Thus, repeated and significant decompression is unlikely to explain observed resorptions. An increase in H_2O content or temperature is a more likely cause. The most feasible process to produce such rapid changes in the growth environment is the movement of the crystal in a melt with a gradient of water content and/or temperature.

Repeated major resorption surfaces associated with an abrupt increase followed by a more continuous decrease in An at a scale of 100 μm may thus be explained by three processes.

1. Crystals move repeatedly in a water concentration gradient towards a more water-rich magma. As water content increases in the melt as a result of crystallisation, this magma will be also cooler and more differentiated. Such a process can be identified using minor and trace elements, as discussed below.
2. Crystals move repeatedly in a gradient towards a hotter, less differentiated magma without any significant changes in water content.
3. The magma chamber is periodically replenished with a hotter, more mafic magma. Only such an event will be recorded in all crystals present in the magma chamber at that time.

To distinguish between hypotheses 2 and 3, we need to find evidence for or against resorptions that are correlated between crystals where slightly different patterns may represent the same event. In our samples the distance from R_1 to the rim, and the degree of resorption in the crystals are indeed similar. This suggests that the R_1 resorption may in fact represent the same event recorded by all three crystals. If the effect of a water gradient can be ruled out (see discussion of trace elements), this observation favours the hypothesis of magma recharge for the R_1 resorption. Minor resorption events that cannot be correlated would then suggest individual convective movement in a thermal and compositional gradient in between and after the prominent resorption event (R_1).

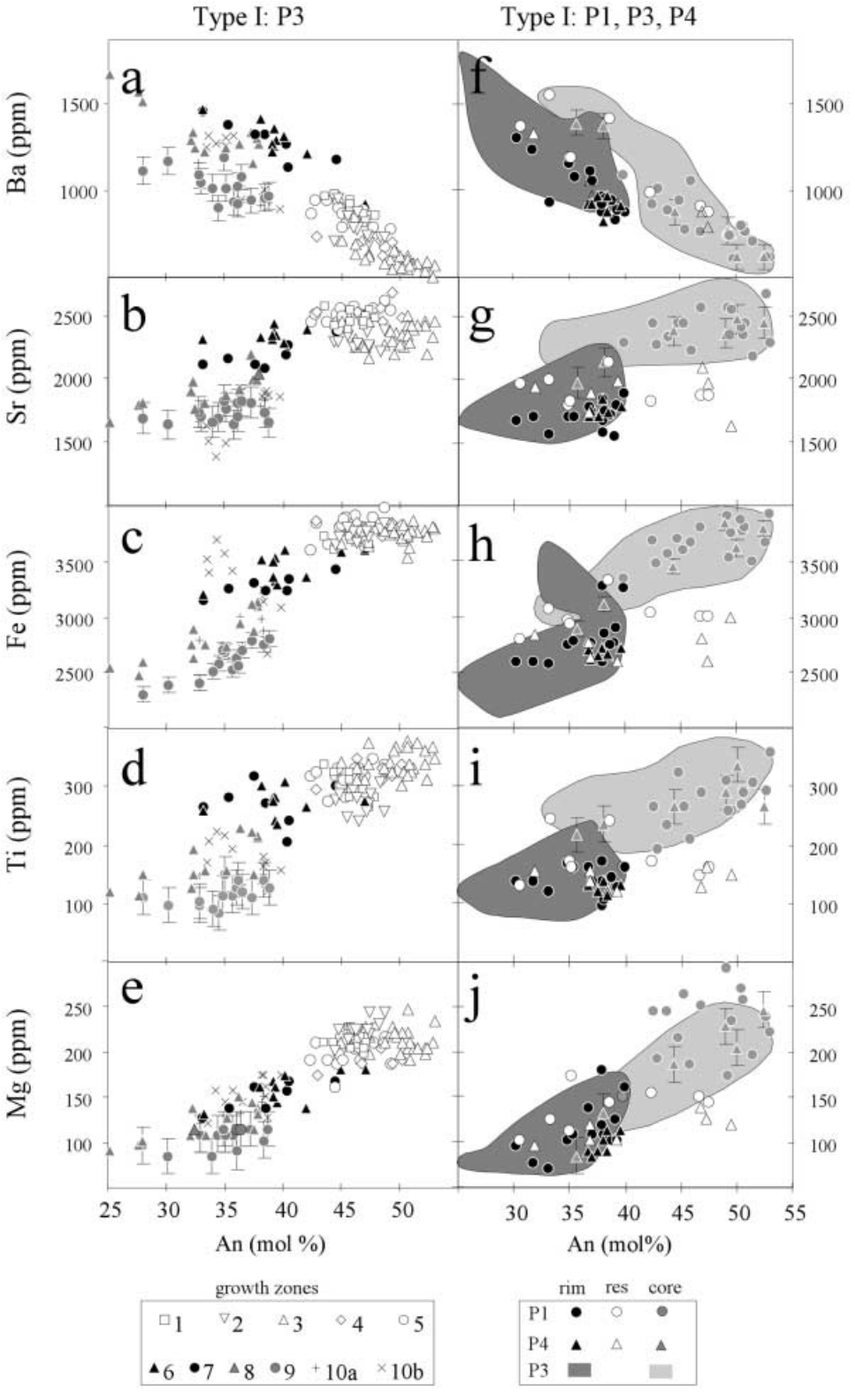

Fig. 5a–j. Trace-element variations vs. An content in plagioclase from Parinacota andesite PAR-130. **a–e** Plagioclase P3. Growth-zone *numbers* correspond to those of Fig. 4a. **f–j** Comparison of crystals P1, P3 and P4, including resorption zones (res). The positive correlation between Fe, Ti and Sr, Mg from core to rim reflects magmatic differentiation. By contrast, the resorption zones seen in Fig. 3 fall off this trend to low Fe, Ti and Sr at high An contents, and probably reflect changes in water content (see discussion in text)

Control on minor and trace elements

When crystals grow near equilibrium, their concentrations in minor and trace elements are controlled by the concentration of these elements in the melt, and the partition coefficients between crystal and melt. In addition, diffusion in the crystal could homogenise initial variations. The role of these factors in our samples is discussed below for the different elements.

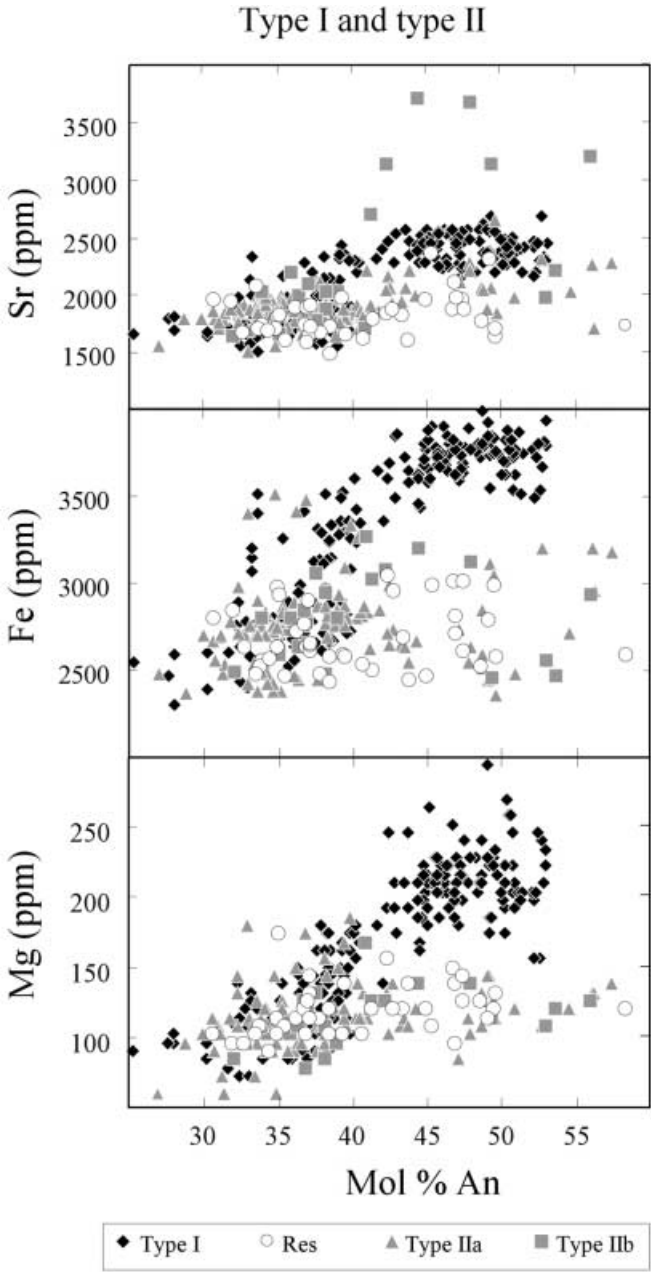

Fig. 6. Sr, Fe and Mg concentrations of all plagioclase crystal types of PAR-130 plotted against anorthite. At high An content, types IIa and IIb both have low Fe contents whereas their Sr contents are low and high respectively

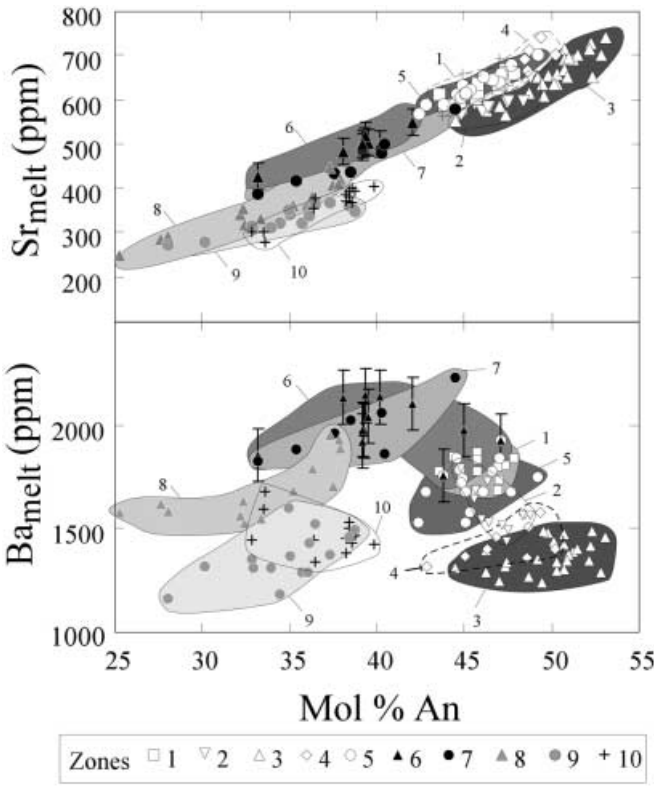

Fig. 7. Calculated melt concentration for Ba and Sr based on element compositions in plagioclase P3 plotted against An content of plagioclase. Concentrations are calculated using the equations of Blundy and Wood (1991) and assuming a temperature of 1,000 °C. Growth-zone *numbers* as in Fig. 5

Partition coefficients

Ba and Sr Blundy and Wood (1991) showed that the dominant factors controlling the partition coefficient (K) of Sr and Ba in plagioclase are the An content of the crystal and temperature, whereas the influence of the major-element composition of the melt is negligible.

The empirical equation of Blundy and Wood (1991) implies that both Ba and Sr become more compatible as the An content of the crystal decreases. As shown in Fig. 5d, e, Ba concentration in the crystal indeed increases, whereas Sr decreases with lower An content. This discrepancy suggests that crystal-chemical control and the effect of variation in melt concentrations are of different importance for these two elements. Crystallisation temperatures are estimated on the basis of the Fe–Ti oxide thermometer (Frost and Lindsley 1991) to range between 850 and 900 °C. Therefore, a temperature change from 1,000 to 850 °C is a reasonable assumption for the crystallisation history. In order to separate crystal-chemical control from other effects, the Ba and Sr concentrations in the melt corresponding to each data point were calculated following Blundy and Wood (1991) for these two temperatures. Differences between calculated melt concentrations at 850 and 1,000 °C are smaller than analytical uncertainty, so that the effect of temperature on Ba and Sr partitioning in our sample can be neglected. The results are shown in Fig. 7, plotted against crystal An content, for a temperature of 1,000 °C. Calculated Ba values (up to 2,200 ppm) are higher than Ba values found in the PAR-130 host rock (Table 2) and in all other Parinacota samples (Wörner et al. 1988; Davidson et al. 1990). This may be partly explained by the uncertainty in the data regression of Blundy and Wood (1991). A data subset containing only their experimental data and including new experimental data of Bindeman et al. (1998) gives a steeper slope and better fit for Ba–temperature

correlations. This would result in lower, more realistic Ba values (=1,600 ppm), consistent with observed bulk-rock compositions. In the following discussion, absolute values must still be considered with caution but general trends may be interpreted. Calculated Ba variations in the liquid are only slightly larger than the uncertainty, and the trend is qualitatively different from that in the crystal. Therefore, the overall Ba variations observed in the crystal reflect crystal-chemical control (An content of the crystal) on the partition coefficient. Effects of other parameters (melt composition, discussed below) are superimposed and subordinate. By contrast, the calculated Sr variations in the liquid are stronger than, and qualitatively similar to the Sr variations observed in the crystal. The resorption zones are an exception where Sr variations reflect crystal-chemical control.

Fe Fe partitioning strongly depends on fO_2 (Longhi et al. 1976; Phinney 1992; Wilke and Behrens 1999; Sugawara 2001). For given P_{H2O}, K_{Fe} is a non-linear function of ΔfO_2 relatively to FMQ; Wilke and Behrens 1999). Partition coefficients range between 0.03 and 0.36 for basalts at one atmosphere (Phinney 1992), and between 0.085 and 0.54 for intermediate compositions under hydrous conditions at 5 kbar (Wilke and Behrens 1999). The data of Bindeman et al. (1998) show a negative correlation of K_{Fe} and An. However, the experiments were done in a narrow range of compositions where An is likely to be directly correlated to temperature. In the data set of Sugawara (2001), the correlation of K_{Fe} is better with temperature than with An. Therefore, D_{Fe} probably more strongly depends on temperature. For fO_2 between FMQ +0 and +2 and a P_{H2O} of more than 5 kbar, K_{Fe} is between 0.19 and 0.05. We adopt an intermediate value of 0.09, which gives a FeO concentration in the melt of 4.1 wt%. The Fe decrease observed in the crystals from core to rim is not related to changes in partition coefficients, because it would imply a strong decrease in fO_2, or an increase in temperature or An. None of these are likely to occur during differentiation. Therefore, the measured Fe content reflects a decrease of Fe concentration in the melt. At the outermost rim, the situation may be different. Cooling related to eruption and possibly an increase in fO_2 will increase K_{Fe} and could explain the observed strong increase of Fe. Another possible explanation involving a kinetic effect due to the formation of a chemical boundary layer at the crystal rim interface is discussed below. The decrease of K_{Fe} predicted for lower P_{H2O} after ascent is not observed and must be compensated by the other effects.

Mg Experimental values of K_{Mg} in plagioclase vary between 0.025 and 0.05, with only very weak correlations with T (Longhi et al. 1976) or An content (Sato 1989; Bindeman et al. 1998). In the following we consider a constant partition coefficient of 0.035. Calculated MgO concentration in the most mafic melt is 1.42 ± 0.5 wt%.

Ti Experimental data for Ti show a clear negative correlation with An, largely independent of T (Bindeman et al. 1998). We approximate this dependence with the equation $\ln K_{Ti} = -1.75 - 0.015 * An$. Calculated Ti concentration in the crystals range between 0.76 ± 0.1% in the core and 0.16 ± 0.02% at the rim.

Diffusion in the crystal

As trace elements diffuse faster in crystals than major elements, their concentration in plagioclase may not reflect the melt composition at the time of growth but may have been affected and homogenised by subsequent diffusion. For andesine compositions at 900 to 1,000 °C, the diffusivity D_{Sr} is in the order of 10^{-19} to 10^{-18} m^2/s (Giletti and Casserly 1994; Cherniak and Watson 1994). The characteristic times for Sr diffusion ($T = L^2/D_{Sr}$) over distances of L = 10 μm and L = 100 μm are in the order of 30 and 3,000 years at 900 °C and between 3 and 300 years at 1,000 °C respectively. Estimated growth rates of plagioclase in natural melts (10^{-8} to 10^{-12} cm/s; Cashman 1990; Davidson and Tepley 1997) imply growth times between 4 months and 3,000 years for a 1-mm crystal. Sr diffusion time and crystal life time are thus in the same order of magnitude. As diffusivities and partition coefficients of Ba sand Sr are known in plagioclase, diffusion in the crystal can be tested for these two elements. If major-element zoning patterns are preserved, the equilibrium concentration of Sr and Ba obtained after diffusion in the crystal should be anticorrelated with An content, because of the An dependence of the partition coefficients (Zellmer et al. 1999). Such trends are indeed observed for Sr in the core of P3, and for Ba over the whole crystal. In order to test whether this is due to diffusion, we consider Sr concentrations in the melt as calculated for Fig. 7 in more detail.

These calculated melt compositions are used here only as a reference, and represent the concentrations of hypothetical melts with which each analysed point of the crystal would have been in equilibrium during growth. Complete diffusive equilibration of Sr would result in uniform calculated Sr concentration in the melt. Partial diffusive equilibration would first affect the small-scale compositional heterogeneities. The smallest growth layers would then have constant Ba and Sr equilibrium melt concentrations at variable An, whereas the compositional variations on a larger scale would remain. Significant variation in Sr in the calculated equilibrium melt concentration occurs at only 50–200 μm scale in zones 1–5. This indicates that, even in the core, Sr variations at this scale have not been totally erased by diffusion. As Ba diffusion is slower (Cherniak 1999), Ba did not diffuse extensively in the core either. The near-equilibrium compositions for Sr and Ba at 500-μm scale in the core are thus not due to diffusive equilibration. Diffusion probably smoothed only smallest (=10 μm) oscillations

and may have reduced the slope in the Sr–An trends for the 50–200 μm growth zones.

Following Zellmer et al. (1999), this result can in turn be used to infer a maximum residence time of the crystal in the magma prior to eruption. In the present case, this maximum plagioclase residence time in the melt is in the order of 3,000 years at 900 °C or only 300 years at 1,000 °C.

Changes in melt composition Observed trace-element variations in the plagioclase that cannot be accounted for by variable partition coefficients or diffusion in the crystal must reflect variations in the trace-element composition of the host melt. Possible causes are differentiation of the magma due to fractional crystallisation, movement in a compositional gradient, or recharge with less differentiated magma. Additionally, kinetic effects may become important at high growth rates, by formation of a chemical boundary layer at the crystal–melt interface. Such a layer would be depleted in plagioclase-compatible elements and enriched in elements incompatible in plagioclase.

Differentiation and mixing with a more differentiated magma The observed decrease in Sr, Fe, Ti, Mg and An content in the plagioclase from core (zone 3) to rim (zone 9) is qualitatively consistent with melt evolution expected for an andesite-dacite magma fractionating plagioclase, pyroxene, Ti–Fe oxides, and small amounts of amphibole.

One possible scenario would be to assume that changes in host melt trace elements are solely caused by crystallisation of the phenocrysts actually present in the rock. In this case, the resorption surfaces would correspond only to physical changes (P, T, water content). The concentration of Sn, Ti, Fe, and Mg in the less differentiated melt (in contact with zone 3 of P3 crystal), calculated using the partition coefficients discussed above, are consistent with an initial melt composition equal to or slightly less differentiated than the whole rock composition. We thus observe only slightly more differentiation of the melt than for closed system, which requires a small amount of either crystal settling or influence of a more differentiated magma. However, most of the Sr decrease calculated for the melt (700 to 450 ppm, depending on the temperature) occurs during the crystallisation of zones 6 and 7, which only represent less than 10% (in volume) of the crystal. This rapid change in Sr is two to three times larger than can be explained by in-situ crystallisation of these plagioclase zones. Singer et al. (1995) interpreted similar observations as kinetic effects by depletion of a boundary layer at the melt–crystal interface due to rapid growth. However, in our case a decrease is also found for Fe, which should have the opposite behaviour if kinetically controlled (see below).

The Ba increase with decreasing An content in zones 6 to 8 is also consistent with the crystallisation of the phases considered above, whereas subsequent decrease in Ba with decreasing An content requires the fractionation of a K- (and Ba-)rich phase such as biotite or sanidine. Sample PAR-130, however, contains no sanidine and rare biotites have resorbed, and rounded shapes suggest that they did not crystallise in this melt. The Ba decrease is also inconsistent with kinetic effects – Ba, if kinetically controlled, should increase.

The change in the degree of differentiation in the host melt as recorded in the crystals therefore cannot be fully explained by their crystallisation. A possible scenario to explain this is progressive mixing with a more differentiated magma. The most plausible origin of such differentiated magma is the boundary layer near the magma chamber wall where cooling and fractional crystallisation takes place. The influence of this boundary layer occurs mostly during the crystallisation of zones 6, 7, and 8 where the decrease in Ba is most pronounced.

Resorption and mixing with a more mafic magma In contrast to An content, trace elements allow the distinction between thermal and chemical causes of resorption. Hammouda et al. (1996), using Sr isotopes in partial dissolution of fluorphlogopite-plagioclase pairs, showed that the response of the plagioclase crystallising just after resorption to chemical changes in the melt is very fast. Thus, in the case of chemical mixing with a less differentiated magma, a trend reverse to differentiation (i.e. towards higher Fe, Ti, Sr and higher An content) is expected in the resorption zone itself as well as in the zones grown subsequently.

Plagioclase growth subsequent to resorption in zones 1 to 3, e.g. after R_1, is characterised by higher An and low Ba although the compositional contrast is low and the resorptions are weak. High An and increasingly lower Ba in zones 1 to 3 (Fig. 4) suggest mixing with successively more mafic magma. As R_1 can be correlated between crystals, this recharge is common for all type I crystals. Regrowth after resorption in these zones is relatively low in Sr at a given An, which is shown by the An–Sr offset (Fig. 5). These observations argue that recharge is by a relatively Sr-poor magma with an otherwise low compositional contrast. Therefore, the recharging magma could correspond to a differentiated equivalent of the Sr-poor mafic Ajata andesite (Ginibre et al. 2001).

The outer growth zones in P3, and in particular zones 7 and 9 immediately outward from the resorption surfaces show high An and trace-element concentrations (Fe, Mg, Sr) which then again decrease until the next resorption surface. This indicates a chemical effect of repeated mixing with mafic magma. The absence of correlation of these resorption surfaces between crystals (see discussion of An content), and the fact that the compositions lie on the differentiation trend suggests that these resorptions, even though they are similar, affected the phenocrysts individually. Therefore, they may be caused by convective movements of crystals in a gradient rather than distinct recharge events.

The resorption zone R_0 in P1 and P4, which is large enough to be analysed, is different. The constant or even lower Fe, Ti, Sr, and Mg concentrations at increasing An content indicate no chemical change in the host melt close to the crystal at the time of resorption. The resorption is thus not due to a bulk chemical change but rather to an increase in temperature and/or H_2O content. On the other hand, when significant dissolution occurs, a boundary layer may form around the crystal in which the melt is enriched in the plagioclase component and its compatible elements such as Sr. Regrowth after resorption in the calcic rim should thus be also enriched in Sr. This is not what we observe, and the low Sr content in the resorption zone shows that this effect is limited. To explain the high An, low Sr regrowth after resorption, two possible explanations remain: (1) a more mafic melt is present, which may bring the necessary heat but its chemical influence is not recorded directly after resorption, and (2) the resorption is due to an increase in water content at otherwise relatively constant melt composition. Because a significantly more mafic composition is not seen in the zones grown subsequently to R_0, in P1 and P4 and in the equivalent zone 8 in P3, the latter hypothesis is more likely.

Crystal margins: kinetic control and changes in partition coefficients The outermost margin of the crystals corresponds to the final stage of crystallisation during or after eruption. It is thus expected to have grown faster at higher cooling rate as well as at lower temperature and pressure than the rest of the crystal. The change in An oscillation mode at the outer rim to narrow and high-amplitude oscillations is typical for this final growth phase.

A chemical boundary layer may form at the crystal–melt interface at high growth rate (Bottinga et al. 1966). Elements which are incompatible in plagioclase (Fe, Ba, Mg, Ti) will be enriched in this layer whereas compatible Sr will be depleted. This can qualitatively explain the increase in Fe, Mg, Ti, and Ba and the decrease in Sr observed in the outermost margin of crystal P3.

However, the effect is very strong for Fe and weak for Mg, which differs from the observations of Bottinga et al. (1966) who reported similar gradients for Mg and Fe in the melt. This suggests the influence of other factors for Fe, where a temperature increase and P_{H2O} decrease cause an increase in Fe partition coefficient. Possibly an increase in fO_2 at this stage also plays a role. These factors have little effect on Ti and Mg, which explains the difference.

Type II crystals

The smaller and more abundant type II plagioclase phenocrysts show low Fe and Mg contents at high An. This can be explained by two processes: (1) lower partition coefficients for Mg and Fe at constant melt composition, or (2) increase in An content of the plagioclase crystallising from a low-Mg and low-Fe differentiated melt due to an increase in water content. Because the influences of physical factors on K_{Fe} and K_{Mg} are different, and K_{Mg} is essentially constant, we conclude that the low Fe and Mg concentrations in the crystals should in fact reflect low concentrations in the melt rather than variable partition coefficients. By implication, this suggests that An-rich zones of these crystals grew in a water-rich differentiated boundary layer.

The variable Sr concentration at high An content reflects the influence of different initial magmas. Type IIa crystals have low Sr concentrations similar to those found in the differentiated parts of type I crystals, suggesting the same parent magma. On the contrary, the higher Sr concentrations of type IIb crystals at relatively differentiated compositions inferred from Mg and Fe indicate an initial magma with significantly higher Sr concentration. Such a magma was in fact erupted from Parinacota volcano in the last Ajata stage. Mixing with this high-Sr magma shortly before eruption is also evidenced in Old Cone samples (Ginibre et al. 2001). In these samples, Sr concentration in the plagioclase grown from the hybrid magma is as high as 4,500 ppm. This is close to what could be expected in plagioclase of An_{50} crystallising from the high-Sr Ajata andesite (5,000 to 6,000 ppm Sr). Type IIb crystals thus represent remaining crystals derived from the differentiation of such a high-Sr magma.

Crystallization history of dacite PAR-130 and magma chamber dynamics

The early growth history of type I crystals in andesite PAR-130 is characterised by successive recharge events of an only slightly more mafic, Sr-poor magma. This recharge magma could be a differentiated equivalent of the Sr-poor mafic andesite end member, which has been identified as one of the parent magmas to Parinacota rocks. Following this, the next growth phase documents increased differentiation and the influence of a water-rich, differentiated melt, possible representing the magma chamber's boundary layer at the cooler wall. Type II crystals have also partly formed in such an environment.

Superimposed on the differentiation trend, quasi-cyclic resorption events followed by a shift in major- and minor-element concentrations toward less differentiated compositions reflect convective movements in a compositional and/or temperature gradient. These movements would be specific to each crystal but zonation and resorption patterns would become successively more similar towards the rim. This indicates the convergence of crystallisation histories. The last resorption R_0 recognised in several type I crystals shows little evidence for a chemical effect of a new mafic magma after resorption. Comparison with type IIa crystals suggests that this resorption may also have been caused by an H_2O increase close to the magma boundary layer. This is consistent with the increased influence of the H_2O-rich boundary

layer towards the end of the crystallisation history in type I crystals.

Type IIa plagioclase crystals derive from a similar parental magma in the boundary layer, whereas type IIb crystals must be older, as represented by cores grown from the high-Sr end-member magma.

Magma chamber structure and dynamics

Our study shows four important aspects of the dynamics of an andesitic/dacitic magma chamber.

1. The zoning patterns in plagioclase record the existence of gradients (thermal, compositional, water content) between a main magma body and a relatively differentiated, crystal-rich boundary layer, containing older crystals. The water gradient implies that the main magma body is not water saturated.
2. Crystallisation occurs both in the main magma body (type I crystals) and in the crystallising boundary layer (type II crystals). The chemical influence of differentiation in the boundary layer is also seen, but less markedly, in type I crystals. This result may be compared with that of Kuritani (1998) who found for a basaltic magma system that the number of crystals from the boundary layer is small compared to that from the main magma body, but the thickness and An contrast of the corresponding growth zones are higher. In our sample the proportion of crystals influenced by the boundary layer is larger (over 50%) but the effect is smaller. This can be explained by the higher viscosity of andesitic/dacitic magmas: only the crystals from the interface of a stable crystal mush and the main magma body may be brought into the main magma body, whereas deeper layers could be sampled by a less viscous basaltic magma. The increasing influence of the boundary layer may indicate an origin near to the roof, and possibly also the influence of liquid differentiation of the melt at the wall, as suggested by Turner (1980) and McBirney et al. (1985).
3. The high frequency of resorption in crystals from the main magma body indicates the role of convection without evidence of significant mafic recharge. The record of compositionally and thermally variable crystallisation conditions requires not only movement of crystals in gradients but also sufficient local mixing. Convection and mixing must also have produced small-scale heterogeneities which persisted over a time sufficiently long for the crystal to grow and to record these variations. This can hardly occur under conditions of laminar convection, as proposed by Singer et al. (1995). It requires some turbulence, even though this is not expected from the viscosities of a dacitic magma. Repeated movement of crystals between different compositional and thermal regimes independent of whole-sale mixing and mafic is a process that we call "convective crystal dispersion".
4. The amount of differentiation recorded in type I plagioclase is only slightly larger than the closed-system differentiation and involves mixing from the differentiated boundary layer. This indicates limited crystal fractionation by settling, and high crystal retention in the magma. Settling and re-entrainment of crystals in a convecting magma body depends on magma viscosity, and high crystal retention is expected only in very viscous magma (Marsh and Maxey 1985; Martin and Nokes 1988; Solomatov et al. 1993; Hawkesworth et al. 2000). However, our results show that the time scale of crystal settling must be large compared to that of melt differentiation by crystallisation.

Time scale of crystallisation and of magma evolution

The dominant differentiation history recorded in type I crystals of sample PAR-130 is at contrast with the data shown by Singer et al. (1995) at San Pedro volcano (central Chile), which clearly show open-system evolution. Temporal constraints from Sr diffusion suggest a differentiation time shorter than a few thousand years. This is close to the time scale calculated by Hawkesworth et al. (2000) for 50% closed-system differentiation of a 10-km^3 magma body releasing heat with a power output of 100 MW. This is consistent with our result that the evolution of PAR-130 after the initial recharge is not very far from closed-system crystallisation.

Growth rates of the crystal from in the main magma body may be calculated from the residence time. The euhedral zone boundaries of crystal P3 suggest repeated but restricted resorption. It is reasonable to assume that the time elapsed between growth episodes is of the order of magnitude of the growth time itself. In this case, the growth of a 2-mm crystal in less than a few hundred or thousand years implies minimum growth rates of 10^{-10} or 10^{-11} cm/s. This is consistent with growth rates reported in the literature (Cashman 1990).

High-Sr type IIb crystals and the low-Sr recharge in type I crystals show the influence, even at low magma recharge rates, of both high-Sr and low-Sr Parinacota magmas. Thus, the two parental magmas documented from volcano evolution and bulk-rock analyses (Wörner et al. 1988) may actually be recorded during plagioclase growth in a single rock sample.

Acknowledgements We thank Jon Davidson and George Bergantz for useful discussions. Kurt Knesel and an anonymous reviewer are acknowledged for their constructive review and thought-provoking critical comments. This study was part of the DFG-funded SFB 468.

References

Allègre CJ, Provost A, Jaupart C (1981) Oscillatory zoning: a pathological case of crystal growth. Nature 294:223–228

Anderson AT Jr (1983) Oscillatory zoning of plagioclases: Nomarski interference contrast microscopy of etched polished sections. Am Mineral 68:125–129

Anderson AT (1984) Probable relations between plagioclase zoning and magma dynamics, Fuego Volcano, Guatemala. Am Mineral 69:660–676

Bindeman IN, Davis AM, Drake MJ (1998) Ion microprobe study of plagioclase – basalt partition experiments at natural concentration level of trace elements. Cosmochim Geochim Acta 62:1175–1193

Blundy JD, Shimizu N (1991) Trace element evidence for plagioclase recycling in calc-alkaline magmas. Earth Planet Sci Lett 102:178–197

Blundy JD, Wood BJ (1991). Crystal-chemical controls on the partitioning of Sr and Ba between plagioclase feldspar, silicate melts, and hydrothermal solutions. Geochim Cosmochim Acta 55:193–209

Bottinga Y, Kudo A, Weill D (1966) Some observation on oscillatory zoning and crystallization of magmatic plagioclase. Am Mineral 51:792–806

Brophy JG, Dorais MJ, Donnelly-Nolan J, Singer B (1996) Plagioclase zonation in hornblende gabbro inclusions from Little Glass Mountain, Medicine Lake volcano, California: implications for fractionation mechanisms and the formation of composition gaps. Contrib Mineral Petrol 126:121–136

Cashman KV (1990) Textural constraints on the kinetics of crystallization of igneous rocks. In: Nicholls J, Russell JK (eds) Modern methods of igneous petrology, understanding magmatic processes. Mineral Soc Am, Washington, DC. Rev Mineral 24:259–314

Cherniak DJ (1999) Ba diffusion in Feldspars. In: AGU Fall Meet 1999, EOS Trans Am Geophys Union 80 suppl 46:F1078

Cherniak DJ, Watson B (1994) A study of diffusion in plagioclase using Rutherford backscattering spectrometry. Geochim Cosmochim Acta 58:5179–5190

Davidson JP, Tepley FJ (1997) Recharge in volcanic system: evidence from isotope profiles of phenocrysts. Science 275:826–829

Davidson JP, MacMillan NJ, Moorbath S, Wörner G, Harmon RS, Lopez-Escobar L (1990) The Nevados de Payachata volcanic region (18°S/69°W, N. Chile) II. Evidence for widespread crustal involvement in Andean magmatism. Contrib Mineral Petrol 105:412–432

Frost BR, Lindsley DH (1991) Occurrence of iron-titanium oxides in igneous rocks. In: Lindsley DH (ed) Oxide mineral: petrologic and magnetic significance. Rev Mineral 25

Giletti BJ, Casserly JED (1994) Strontium diffusion kinetics in plagioclase feldspars. Geochim Cosmochim Acta 58:3785–3793

Ginibre C, Kronz A, Wörner G (2002) High-resolution quantitative imaging of plagioclase composition using accumulated back-scattered electron images: new constraints on oscillatory zoning. Contrib Mineral Petrol 142:436–448

Ginibre C, Wörner G, Kronz A (2001) Magma chamber processes reflected in major, minor and trace element plagioclase zoning (Parinacota volcano, Chile). J Conf Abstr 6:807

Grove TL, Baker MB, Kinzler RJ (1981) Coupled CaAl-NaSi diffusion in plagioclase feldspar: Experiments and application to cooling rate speedometry. Geochim Cosmochim Acta 58:2113–2121

Hammouda T, Pichavant M (2000) Melting of fluorophlogopite-plagioclase pairs at 1 atmosphere. Eur J Mineral 12:315–328

Hammouda T, Pichavant M, Chaussidon M (1996) Isotopic equilibration during partial melting: an experimental test of the behavior of Sr. Earth Planet Sci Lett 144:109–121

Hawkesworth CJ, Blake S, Evans P, Hughes R, Macdonald R, Thomas LE, Turner SP, Zellmer G (2000) Time scales of crystal fractionation in magma chambers – integrating physical, isotopic and geochemical perspectives. J Petrol 41:991–1006

Housh TB, Luhr JF (1991) Plagioclase-melt equilibria in hydrous system. Am Mineral 76:477–492

Huppert HE, Turner JS (1991) Comment on 'On convective style and vigor in sheet like magma chambers' by Bruce D. Marsh. J Petrol 32:851–854

Johannes W, Koepke J, Behrens H (1994) Partial melting reactions of plagioclases and plagioclase bearing systems. In: Parson I (ed) Feldspars and their reactions. Kluwer, Dordrecht, pp 161–194

Kuritani T (1998) Boundary layer cristallization in a basaltic magma chamber: Evidence from Rishiri Volcano, northern Japan. J Petrol 39:1619–1640

Lasaga AC (1982) Toward a master equation in crystal growth. Am J Sci 282:1264–1288

L'Heureux I, Fowler AD (1996) Isothermal constitutive undercooling as a model for oscillatory zoning in plagioclase. Can Mineral 34:1137–1147

Lofgren GE (1974) An experimental study of plagioclase crystal morphology: isothermal crystallization. Am J Sci 274:243–273

Longhi J, Walker D, Hays JF (1976) Fe and Mg in plagioclase. In: Proc 7th Lunar Sci Conf, pp 1281–1300

Loomis TP (1982) Numerical simulations of crystallization processes of plagioclase in complex melts: the origin of major and oscillatory zoning in plagioclase. Contrib Mineral Petrol 81:219–229

Marsh BD (1989a) Magma chambers. Annu Rev Earth Planet Sci 17:439–474

Marsh BD (1989b) On convective style and vigor in sheet like magma chambers. J Petrol 30:479–530

Marsh BD, Maxey MR (1985) On the distribution and separation of crystals in convecting magma. J Volcanol Geotherm Res 24:95–150

Martin D, Nokes R (1988) Crystal settling in a vigorously convecting magma chamber. Nature 332:534–536

McBirney AR, Baker BH, Nilson RH (1985) Liquid fractionation. Part I. Basic principles and experimental simulations. J Volcanol Geotherm Res 24:1–24

Nakamura M, Shimakita S (1998) Dissolution origin and syn-entrapment compositional changes of melt inclusions in plagioclase. Earth Planet Sci Lett 161:119–133

Nelson ST, Montana A (1992) Sieve-textured plagioclases in volcanic rocks produced by rapid decompression. Am Mineral 77:1242–1249

Nixon GT, Pearce TH (1987) Laser-interferometry study of oscillatory zoning in plagioclase: The record of magma mixing and phenocryst recycling in calc-alkaline magma chambers, Iztaccíhuatl Volcano, Mexico. Am Mineral 72:1144–1162

Pearce TH, Russel, JK, Wolfson I (1987) Laser-interference and Nomarski interference imaging of zoning profiles in plagioclases phenocrysts from the May 18, 1980, eruption of Mount St. Helens, Washington. Am Mineral 72:1131–1143

Phinney WC (1992) Partitioning coefficients for iron between plagioclase and basalt as a function of oxygen fugacity: implications for Archean and lunar anorthosites. Geochim Cosmochim Acta 56:1885–1895

Sato H (1989) Mg-Fe partitioning between plagioclase and liquids in basalts of Hole 504B, ODP leg 111: a study of melting at one atm. College Station, TX, Proc Ocean Drilling Program Sci Res 111:17–26

Singer B, Dungan MA, Layne GD (1995) Textures and Sr, Ba, Mg, Fe, K, and Ti compositional profiles in volcanic plagioclase: Clues to the dynamics of calc-alkaline magma chambers. Am Mineral 80:776–798

Solomatov VS, Olson P, Stevenson DJ (1993) Entrainment from a bed of particles by thermal convection. Earth Planet Sci Lett 120:387–393

Sugawara T (2001) Ferric iron partitioning between plagioclase and silicate liquid: thermodynamics and petrological applications. Contrib Mineral Petrol 141:659–686

Tepley FJ III, Davidson JP, Tilling RI, Arth JG (2000) Magma mixing, recharge and eruption histories recorded in plagioclase phenocrysts from El Chichón Volcano, Mexico. J Petrol 41:1397–1411

Tsuchiyama A (1985) Dissolution kinetics of plagioclase in the melt of system diopside-albite-anorthite, and origin of dusty plagioclases in andesites. Contrib Mineral Petrol 89:1–16

Turner JS (1980) A fluid-dynamical model of differentiation and layering in magma chambers. Nature 285:213–215

Wilke M, Behrends H (1999) The dependence of the partitioning of iron and europium between plagioclase and hydrous tonalitic melt on oxygen fugacity. Contrib Mineral Petrol 137:102–114

Wörner G, Harmon RS, Davidson J, Moorbath S, Turner DL, McMillan N, Nye C, Lopez-Escobar L, Moreno H (1988) The Nevados de Payachata volcanic region (18°S/69°W, N. Chile). I. Geological, geochemical, and isotopic observations. Bull Volcanol 50:287–303

Wörner G, Hammerschmidt K, Henjes-Kunst F, Lezaun J, Wilke H (2000) Geochronology ($^{40}Ar/^{39}Ar$, K-Ar, and He-exposure-) ages of cenozoic magmatic rocks from Northern Chile(18°-20°S): Implications for magmatism and tectonic evolution of the central Andes. Rev Geol Chile 27:205–240

Zellmer GF, Blake S, Vance D, Hawkeswoth C, Turner S (1999) Plagioclase residence times at two island arc volcanoes (Kameni Islands, Santorini, and Soufriere, St. Vincent) determined by Sr diffusion systematics. Contrib Mineral Petrol 136:345–357